An Atomic Beam Polarimeter to Measure the Nuclear Polarization in the HERMES Gaseous Polarized Hydrogen and Deuterium Target

C. Baumgarten [a] B. Braun [a,b] G. Court [d] G. Ciullo [e] P. Ferretti [e] A. Golendukhin [b,ℓ,k] G. Graw [a] W. Haeberli [c] M. Henoch [b] R. Hertenberger [a] N. Koch [b] H. Kolster [a,f,j] P. Lenisa [e] A. Nass [b] S.P. Pod'yachev [b,h] D. Reggiani [e] K. Rith [b] M.C. Simani [g] E. Steffens [b] J. Stewart [d,i] T. Wise [c]

[a] *Sektion Physik, Ludwigs-Maximillians-Universität München, 85748 Garching, Germany*

[b] *Physikalisches Institut, Universität Erlangen-Nürnberg, 91058 Erlangen, Germany*

[c] *Department of Physics, University of Wisconsin-Madison, Madison, Wisconsin 53706, USA*

[d] *Physics Department, University of Liverpool, Liverpool L69 7ZE, United Kingdom*

[e] *Istituto Nazionale di Fisica Nucleare and Universita', 44100 Ferrara, Italy.*

[f] *Nationaal Instituut voor Kernfysica en Hoge-Energiefysica (NIKHEF), 1009 DB Amsterdam, The Netherlands*

[g] *Department of Physics and Astronomy, Vrije Universiteit, 1081 Amsterdam, The Netherlands*

[h] *Institute of Automation and Electrometry of SB RAS, Russia*

[i] *DESY Zeuthen, 15738 Zeuthen, Germany*

[j] *Current address: Laboratory for Nuclear Science, Massachusetts Institute of Technology, Cambridge, Massachusetts 02139, USA*

[k] *Current address: ATI Technologies Inc., 55 Commerce Valley Dr. W. Thornhill, ON L3T 7V9, Canada*

[ℓ] *Yerevan Institute, 375036, Yerevan, Armenia*

Abstract

An atomic beam polarimeter for measurement of the hyperfine population numbers and the absolute polarization of thermal atomic hydrogen (H) and deuterium (D) beams is described. The principle of measurement and the method of calibration are given. The polarimeter measures the 4 (6) relative hyperfine population numbers of

a thermal H (D) beam in the region of 10^{13} atoms/s to an absolute error of less than 0.01. The polarimeter has been in continuous operation with the internal polarized hydrogen and deuterium gas target used in the HERMES experiment at DESY since 1996.

Key words: Polarized Targets, Polarimeters, Detection of Atomic Beams, Spin-polarized Hydrogen, Hyperfine Interactions
PACS: 29.25.P, 07.60.F, 07.77, 67.65, 31.30.G

---

1 Introduction

The HERMES experiment at DESY has a program to make high precision measurements on nucleon spin structure functions by studying the deep inelastic scattering of 27.5 GeV polarized electrons (or positrons) from nuclear polarized hydrogen and deuterium targets [1,2]. The polarized electron (positron) beam in the storage ring is used in conjunction with an internal gaseous polarized target. The polarized nucleons for the target are produced in the form of a beam of approximately $6.4 \cdot 10^{16}$ atoms sec^{-1} in an atomic beam source (ABS). This beam is injected into the center of a storage cell which is an open ended tube mounted so that the electron beam passes along its axis. The injected atoms collide with the walls of the cell which is cooled, and then diffuse into the storage ring beam pipe where they are removed by a high capacity pumping system. This produces a triangular atom density profile along the electron beam path. The cooling reduces the atom velocity and maximizes the atom residence time in the interaction region. This technique allows the production of a usable target thickness of up to 10^{14} nucl cm^{-2}. The effective polarization of this target is obtained by measuring the polarization of a sample of atoms effusing from a side tube connected to the center of the cell with an atomic beam polarimeter. This type of polarimeter has been given the name Breit-Rabi Polarimeter (BRP) [3]. The requirements for this polarimeter are firstly that it should be able to measure the absolute value of the polarization of both nuclei and electrons in the sample beam with a systematic uncertainty of better than 2 %. An absolute measurement is required because there are no electron beam associated nuclear reactions which can be used to measure or calibrate the target polarization. Secondly, the statistical error should allow a significant measurement to be made in a time period of approximately one minute to be compatible with fast reversal of the target spin direction.

The calculation of the target polarization as seen by the HERA beam passing through the cell involves the density weighted average of the polarization of the atoms along the cell axis. The relationship between the polarization of the sampled atoms and the polarization of the entire target requires the determination of a sampling correction which involves a detailed analysis of the

diffusion of the atoms through the cell [4,17]. Additionally account must be taken of the possibility of atom-atom recombination occurring during wall collisions, which requires a measurement of the molecular fraction in the sample beam. This is done with a gas analysis system (TGA).

An early version of this type of polarimeter has been described in 1992 [3], where arguments on the choice of the method and a preliminary version of the measurement technique can be found.

2 Principle of Operation of the Polarimeter

The design goal of the polarimeter is to precisely measure the relative populations N_i of the hyperfine states (hfs) of a thermal atomic H or D beam of low intensity. The nuclear and electronic polarizations of the atoms in a given magnetic field are linear functions of the N_i and are calculated as described in Sec. 4 [5]. The labeling of the hyperfine states follows the notation in the same reference. The energy level diagram of hydrogen is shown in Fig. 1.

The polarimeter has three main components, a sextupole magnet system which operates as an electron spin filter, adiabatic rf-transitions which exchange the hfs populations of two or more hfs states and a beam detection system. In the sextupole system, which contains two magnets, the Stern-Gerlach force acts on the magnetic moment of the uncoupled electron focusing (defocusing) atoms with the magnetic quantum number $m_J = \frac{1}{2}$ ($m_J = -\frac{1}{2}$) [5–7]. Two adiabatic rf-transition units [5] mounted in front of this sextupole system enable the exchange of the hfs populations of two (or more) hyperfine states with an efficiency of typically more than 90 %. This permits selection of different combinations of initial hyperfine states that are able to reach the detector.

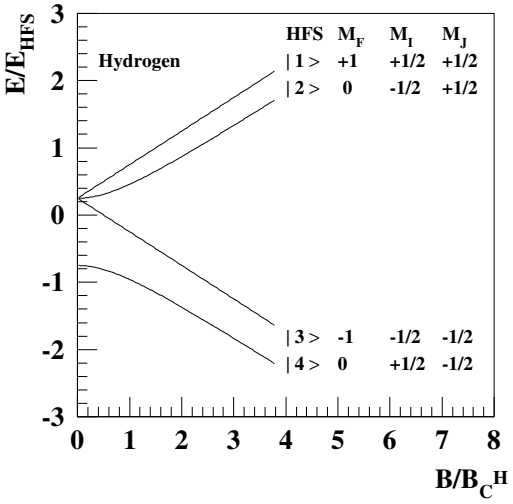

Fig. 1. Energy level diagram of the hyperfine states of hydrogen as function of the magnetic holding field. The hfs population of state $|\, i \,\rangle$ is N_i.

Fig. 2 illustrates the principle for a hydrogen beam with two transitions in operation (The terms *SFT* and *MFT* are explained in Sec. 3.2). This principle applies also to deuterium.

A series of subsequent beam intensity measurements with different combinations of rf-transitions in use gives data that are described by a linear system of equations from which the relative hfs population numbers N_i are calculated.

3 The Experimental Apparatus

The HERMES storage cell is a 400 mm long, 75 μm thick pure aluminum tube of elliptical crossection (9.8 $\times$ 29 mm in diameter) [8]. It is coated with Drifilm [9] in order to minimize spin relaxation and atomic recombination when wall collisions occur. The storage cell is mounted on rails which can be cooled with He gas down to temperatures in the region of 30 K. The rails are cantilever mounted to the upstream flange of the target vacuum chamber. A super-conducting solenoid magnet which is mounted externally to the target chamber provides a homogeneous field of up to 350 mT parallel to the HERA beam direction. The field defines the nucleon spin direction and suppresses nucleon depolarization processes by decoupling them from the electrons.

The spin polarized hydrogen or deuterium atoms produced in the ABS [10] are ballistically injected into the storage cell center via a side tube (*injection tube*) of 10 mm diameter and 100 mm as shown in Fig. 3. A second side tube (*sample tube*, 5 mm diameter, 100 mm length) also attached to the storage cell center allows a small fraction of the atoms to enter the acceptance of the polarimeter. The axis of both ABS and BRP are tilted by 30 ° with respect to the horizontal plane to ensure the atoms sampled by the BRP have made at least one wall collision and so are in thermal equilibrium with the cell (see

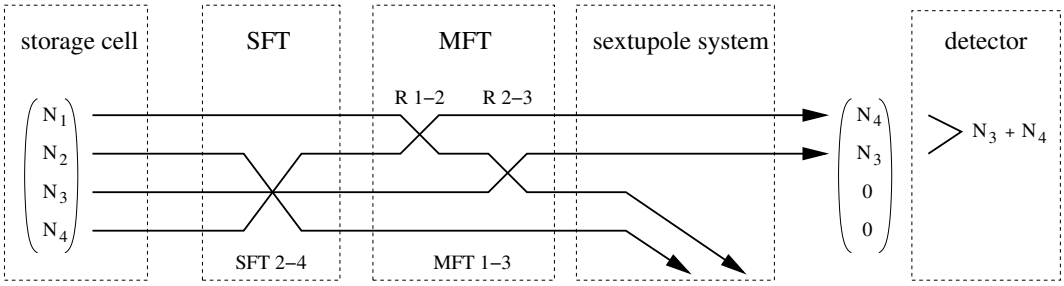

Fig. 2. Principle of operation of the polarimeter: In a first step adiabatic rf-transitions allow to exchange the population of the hyperfine states (here SFT 2-4 and MFT 1-3, composed of the two steps R 1-2 and R 2-3). The following sextupole system acts as a filter and removes half of the hfs states with $m_J = -1/2$ from the beam. The signal in the detector is proportional to the sum of the populations of the remaining hfs states with $m_J = +1/2$.

Fig. 3). This is necessary to avoid correlations between the velocity and the spin state of the atoms. Such correlations could bias the effect of the sextupole spin filter.

The sample tube is extended by another tube (10 mm diameter, 120 mm length, see Fig. 3) in order to form a sample beam for the TGA. The TGA is mounted at an angle of about 7° with respect to the BRP axis to avoid interference with the sample beam entering the BRP. Both ABS and BRP can be isolated from the target chamber vacuum by valves for maintenance purposes and for setting up. The vacuum system of the BRP is shown in Fig. 4. It is a two stage differential pumping system and has been described in [3,12]. These stages are separated by a small diameter bellows with a low conductance which allows a very low operating pressure in the detection chamber and minimizes the background due to residual gas atoms.

3.1 The Beam Detector

The detector consists of a crossed-beam ionizer in combination with a quadrupole mass spectrometer (Balzers QMA 430) and a channel electron multiplier for single ion detection. A mechanical beam chopper operating at a frequency of approximately 5.5 Hz is mounted in front of the detector (Fig. 3) and allows a background subtraction to be made. The count rates are measured with a time resolving counter (TRC) with 2048 bins. A time-resolved count rate spectrum is shown in Fig. 5. The bin length is adjustable and typically set to 175 μsec. The counts of 16 to 32 chopper periods are summed up for a beam

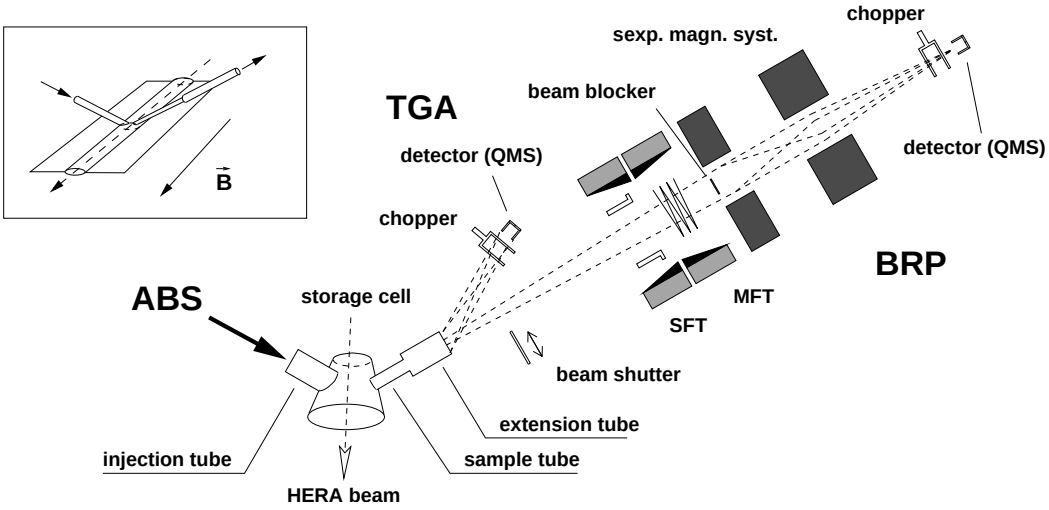

Fig. 3. The setup of the Breit-Rabi type polarimeter (BRP) in the HERMES environment. Both the ABS and BRP axis are tilted by 30° with respect to the horizontal plane. The chamber between BRP and storage cell contains the TGA, consisting of a beam chopper and a quadrupole mass spectrometer (QMS) [11].

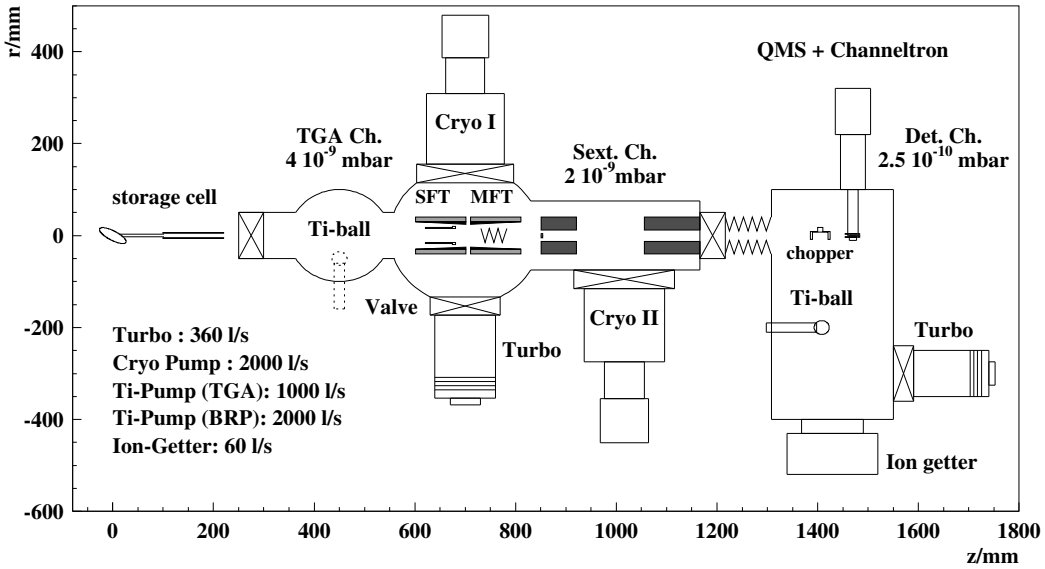

Fig. 4. Schematic of the vacuum system of the BRP. The titanium ball in the TGA chamber is placed in a separate chamber about 30 cm from the beam axis. The indicated pressures are typical for target operation with polarized deuterium.

intensity measurement. The atom count rates of the detector can be affected by the presence of H_2O and H_2 in the beam. The partial pressures of both gases in the sextupole system produce chopped beam in the detection chamber, resulting in a chopped mass 1 background due to dissociative ionization of these molecules. The beam rates of the masses 2 and 18 amu are therefore also measured and used to make corrections to the atomic hydrogen beam measurement. The correction constants are determined by varying the partial pressures of H_2O and H_2 during a warmup of the cryogenic pumps in the first chamber with the gate valves opened.

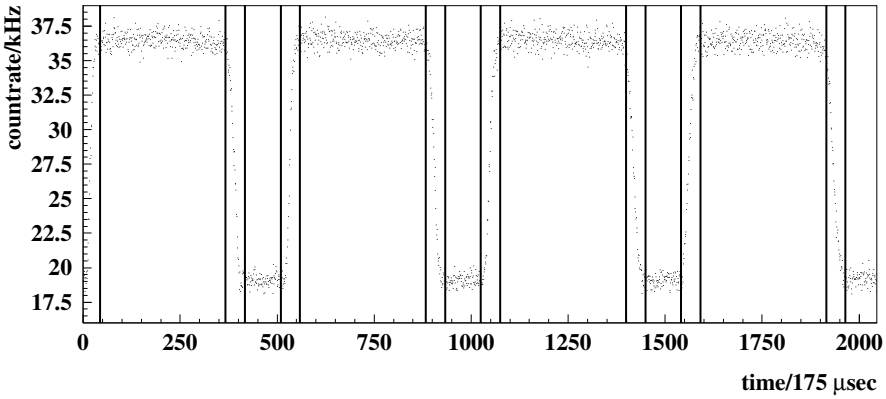

Fig. 5. Time spectrum of atomic count rates in the BRP detector. The vertical lines indicate the limits between the chopper positions *open*, *undefined* and *closed*.

The determination of these corrections is more difficult for deuterium since there are many more channels for dissociative ionization. Thus a beam shutter was installed at the entrance of the BRP, which allows the atomic beam to be switched on and off rapidly by remote control. This enabled a measurement of the correction data to be made with each measurement of the polarization.

3.2 The High Frequency Transition Units

A basic description of transition units is given in [3]. If J, I and F are the quantum numbers of the electron, nuclear and total spin respectively, then a transition with $\Delta F = \pm 1$ is described as a strong field transition (SFT) and with $\Delta F = 0$ as a medium field transition (MFT) [13]. In the current setup two transition units are used, the first is a SFT and the second is a MFT.

The SFT unit uses a resonator cavity with tilted rods [12], so that rf-field components are generated both parallel and perpendicular to the static magnetic field direction (see Fig. 6). Two types of transitions are possible depending on the orientation of the static field B_0 and the rf-field B_1. The *σ-transitions* with $\Delta m_F = 0$ require a parallel field orientation and *π-transitions* with $\Delta m_F = \pm 1$ a perpendicular orientation [14–16]. Thus the use of tilted rods allows both transition types to be induced with the same resonator cavity. The resonance frequency of the cavity can change slightly due to thermal drifts and therefore it is kept in resonance by a feed back loop using the signal from a pickup coil inside the cavity [12]. The frequencies required for hydrogen (1440 MHz) and deuterium (370 MHz) differ and therefore the cavities have to be exchanged when the atom species is changed.

MFT transitions are always π-transitions due to the hyperfine structure, so the high frequency field can be generated by a solenoid coil oriented parallel to the beam axis [13]. A Collins filter is mounted outside the vacuum chamber, but close to the transition unit, in order to provide good matching to the rf-source [12]. The MFT unit can be used both for hydrogen (90 MHz) and deuterium (25 MHz).

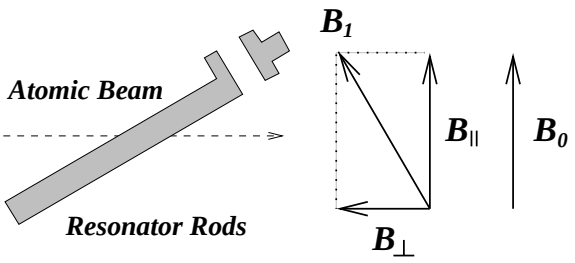

Fig. 6. Schematic side view of the field orientations inside the SFT cavity along the beam axis. Due to the angle between the static field direction (B_0) and the resonator rods, the magnetic rf-field B_1 has both, a parallel ($B_{||}$) and a perpendicular ($B_{\perp}$) component.

3.3 The Sextupole Magnet System

The transition units are followed by a system with two sextupole magnets made of NdFeB permanent magnetic material [7]. The sextupoles have an inner bore of 25 mm diameter and a pole-tip field of 1.45 T. The first is 70 mm and the second 110 mm long with a separation of 135 mm. A beam blocker with a diameter of 9.5 mm is mounted on axis at the entrance of the first sextupole magnet. This ensures that no atoms with $m_J = -\frac{1}{2}$ can pass through the system close to the axis where the Stern-Gerlach force on the atoms is small.

4 Calculation of Polarization

The hfs states of are labeled in the order of the energy levels [5] as shown for hydrogen in Fig. 1. If σ_a is the probability of atoms in hyperfine state $|\, a \,\rangle$ to pass the sextupole system, the count rate in the detector S_{off} with all rf-transition units switched off is

$$S_{off} = c \sum_a \sigma_a \, I_a \,, \tag{1}$$

where I_a is the sample beam intensity of atoms in hyperfine state $|\, a \,\rangle$ and the factor c represents the geometrical acceptance and detection efficiency of the mass spectrometer. If a transition i is switched on the population of two hyperfine states is exchanged and the count rate S_i is given by:

$$S_i = c \sum_b \left(\sum_a \sigma_a \, T^i_{ab} \right) I_b \,, \tag{2}$$

where the matrix T^i_{ab} describes the exchange of the hyperfine states with transition i. In case of the SFT 1-4 for hydrogen the matrix T^{S14}_{ab} has the form:

$$T^{S14} = \begin{pmatrix} 1-\varepsilon_{s14} & 0 & 0 & \varepsilon_{s14} \\ 0 & 1 & 0 & 0 \\ 0 & 0 & 1 & 0 \\ \varepsilon_{s14} & 0 & 0 & 1-\varepsilon_{s14} \end{pmatrix} , \tag{3}$$

with the transition efficiency ε_{s14}. The rules for the classification of the different efficiencies are given is Sec. 4.3. The detector count rates S_i are described

by a set of linear functions of the intensities I_a

$$S_i = c \sum_a M_{ia} I_a \,, \tag{4}$$

where M_{ia} is the *measurement matrix*

$$M_{ia} = \sum_b \sigma_b \, T^i_{ba} \,, \tag{5}$$

which depends on the transition efficiencies and the transmission probabilities for the hyperfine states. In case of the SFT 1-4 count rate, the corresponding expression for Eqn. 4 is given by:

$$\begin{aligned} S_{14} = c \, \{ \, [\, \sigma_1 \, (1 - \varepsilon_{s14}) + \sigma_4 \, \varepsilon_{s14}] \, I_1 + \sigma_2 \, I_2 + \sigma_3 \, I_3 \\ + \, [\, \sigma_4 \, (1 - \varepsilon_{s14}) + \sigma_1 \, \varepsilon_{s14} \,] \, I_4 \, \} \; . \end{aligned} \tag{6}$$

In the ideal case ($\sigma_1 = \sigma_2 \simeq 1$, $\sigma_3 = \sigma_4 \simeq 0$ and $\varepsilon_{s14} \simeq 1$), the equation simplifies to:

$$S_{14} \simeq c \, (I_2 + I_4) \,. \tag{7}$$

The system of linear equations (4) can be solved using four different beam rates S_i in case of hydrogen and six in case of deuterium, if the measurement matrix M_{ia} is defined. This requires knowledge of the efficiencies and the transmission probabilities entering the matrix.

The intensities I_a are calculated by the inverse matrix $R = M^{-1}$:

$$I_a = c^{-1} \sum_b R_{ab} \, S_b \,. \tag{8}$$

If the number of measured count rates with different combinations of rf-transitions is greater than the number of unknowns, the use of the *pseudo-inverse* matrix

$$R = (M^T G_S M)^{-1} M^T G_S \tag{9}$$

is equivalent to a least square fit of the intensities I_b to the measured count rates S_a, where G_S is the inverse covariance matrix of the count rates [19]. The total intensity I_{tot} can then be calculated by the sum over all hyperfine

states $I_{tot} = \sum_a I_a$. The hfs population numbers N_a of the beam are obtained by a normalization of the calculated intensities:

$$N_a = \frac{I_a}{I_{tot}} \,. \tag{10}$$

The polarization of electrons (P_e) and nuclei (P_z and P_{zz}) of the mixed hyperfine states depends additionally on the magnetic field and can be calculated using the normalized expectation values of the corresponding spin operators. For hydrogen the calculation yields

$$\begin{aligned} P_e &= N_1 - N_3 + (N_2 - N_4)\cos 2\theta \\ P_z &= N_1 - N_3 - (N_2 - N_4)\cos 2\theta \,. \end{aligned} \tag{11}$$

and for deuterium [5]

$$\begin{aligned} P_e &= N_1 - N_4 + (N_2 - N_6)\,\cos 2\theta_+ + (N_3 - N_5)\,\cos 2\theta_- \\ P_z &= N_1 + N_6 - N_3 - N_4 + (N_2 - N_6)\sin^2\theta_+ + (N_3 - N_5)\,\sin^2\theta_- \\ P_{zz} &= N_1 + N_4 - N_2\,\tfrac{1}{2}(3\,C_+ + 1) + N_3\,\tfrac{1}{2}(3\,C_- - 1) \\ &\quad - N_5\,\tfrac{1}{2}(3\,C_- + 1) + N_6\,\tfrac{1}{2}(3\,C_+ - 1)\,, \end{aligned} \tag{12}$$

where $C_\pm = \cos 2\theta_\pm$ and the mixing angles θ and $\theta_\pm$ are functions of the holding field B defined by

$$\tan 2\theta = B_C^H / B \qquad \tan 2\theta_\pm = \tfrac{\sqrt{8}}{3B/B_C^D \pm 1} \,. \tag{13}$$

$B_C^H = 50.7\,\mathrm{mT}$ and $B_C^D = 11.7\,\mathrm{mT}$ are the values of the critical field of hydrogen and deuterium respectively [5]. These equations can be written in matrix form for hydrogen

$$(P_e, P_z)^T = M_P^H\,(N_1, N_2, N_3, N_4)^T \;, \tag{14}$$

and deuterium

$$(P_e, P_z, P_{zz})^T = M_P^D\,(N_1, N_2, N_3, N_4, N_5, N_6)^T \;, \tag{15}$$

which simplifies the calculation of the uncertainties.

4.1 The Statistical Uncertainty of the Polarization Measurement

If the statistical uncertainties of the BRP beam rates S_i are given by the - diagonal - covariance matrix C_S, then the covariance matrix C_I of the intensities I_a is given by

$$C_I = R\, C_S\, R^T = \left(M^T C_S^{-1} M\right)^{-1} . \tag{16}$$

The covariance matrix C_N of the occupation numbers N_a is given by

$$(C_N)_{ab} = \sum_{cd} \left(\frac{\partial N_a}{\partial I_c}\right) (C_I)_{cd} \left(\frac{\partial N_b}{\partial I_d}\right) . \tag{17}$$

The partial derivatives are calculated using Eqn. 10

$$\frac{\partial N_a}{\partial I_c} = \frac{I_{tot}\,\delta_{ac} - I_a}{I_{tot}^2} , \tag{18}$$

with δ_{ac} being the Kronecker delta symbol. Finally the covariance matrix C_P of the polarization vector is obtained

$$C_P = M_P^{H,D}\, C_N\, (M_P^{H,D})^T . \tag{19}$$

The statistical error ΔI_{tot} of the total intensity I_{tot} equals the sum over all elements of the covariance matrix C_I:

$$\Delta I_{tot} = \sum_{ab} (C_I)_{ab} . \tag{20}$$

The sextupole transmissions enters into the intensity $I_{\rm tot}$, so that $I_{\rm tot}$ depends on the temperature of the source, i.e. the storage cell. However due to normalization (Eqn. 10) only the ratios of the transmission probabilities of the transmitted hyperfine states are required for the evaluation of the hfs population and the polarization. The method of measuring these ratios is presented in Sec. 4.2.

4.2 The Absolute Calibration of the Polarimeter

The calibration requires the determination of the efficiencies of all transitions as well as a determination of the transmission probabilities of the sextupole

system. The system of equations defined by Eqn. 4 can be made overdetermined because there are more different combinations of high frequency transitions than hfs states. Therefore it is possible to determine additional parameters like efficiencies or sextupole transmissions by making a fit to the data. Since the number of unknowns that can be determined this way is still less than the number of efficiencies, the information of several measurements with different hyperfine populations has to be combined. The HERMES ABS is designed to deliver beams with different combinations of hyperfine populations by switching rf-transitions in the ABS. It is possible to produce beams with nuclear polarization in either direction (P_{z+} and P_{z-}) and no electron polarization (P_e) or alternatively, with electron polarization and no nuclear polarization. The effectiveness of this calibration technique was successfully tested by making measurements with the efficiency of selected transitions being intentionally degraded using reduced rf drive amplitudes.

4.3 Determination of the Transition Efficiencies

The notation used for the efficiencies is in the form of a subscript to ε where s stands for a strong and m for a medium field transition. Since the MFT drives more than one sub-transition denoted by the letter r, e.g. 1-2 and 2-3 in case of hydrogen (1-2, 2-3 and 3-4 in case of deuterium), the description of a MFT requires 2 or 3 efficiencies for hydrogen and deuterium respectively [12]. The order in which these sub-transitions are applied to the beam depends on the sign of the gradient field and yields different effects on the hfs population if it is changed. Here a negative gradient along the beam direction has to be chosen, so that the 1-2 sub-transition appears first. The index of the efficiencies therefore has to be extended and the 1-2 (2-3) sub-transition of the MFT 1-3 is given as ε_{m13r12} (ε_{m13r23}). Accordingly, three efficiencies are required for the description of the MFT in case of deuterium. Since the magnetic field values at which these sub-transitions occur for a given frequency have a very small separation, the efficiency of the nominally off sub-transition may not be zero. Thus all possible MFT sub-transitions have to be included in the calibration procedure.

Two SFT transitions exist in case of hydrogen, described by ε_{s14} and ε_{s24} and 5 in case of deuterium, described by ε_{s16}, ε_{s26}, ε_{s35}, ε_{s25r25} and ε_{s25r36}. The efficiency ε_{s25r36} is expected to be lower than other transitions due to low value of the matrix element related to this transition.

Due to the close proximity of the two transition units there is some cross talk between their magnetic fields. This means that the setting of the static field of the SFT unit changes the field of the MFT unit by a small amount, so that the current of the static field coil of the MFT must be chosen separately for

each SFT setting [20]. Separate efficiencies of the MFT transitions need to be determined for each SFT setting as the transition efficiencies depend on the exact field. The notation for MFT efficiencies therefore requires an extension of the subscript by the letter c (for *c*alibration) and two digits indicating the SFT field used. For example $\varepsilon_{m13r12c14}$ ($\varepsilon_{m13r12c24}$) describes the efficiency of the 1-2 exchange of the MFT 1-3 transition where the SFT fields (static and gradient field) are set to the values of the SFT 1-4 (SFT 2-4). The influence of the MFT field on the strong field transition is small and therefore neglected.

The total number of efficiencies N_{eff} which need to be determined is 10 in case of hydrogen and 41 in case of deuterium. These large numbers are necessary because of the crosstalk between the magnetic fields of the transition units. The number of different transition states of the BRP and thus measurable count rates N_{BRP}, is 11 for hydrogen and 29 for deuterium. If the crosstalk could be avoided, only 6 efficiencies would be required for hydrogen and 14 for deuterium with the corresponding numbers for the count rates being 9 and 20.

If the ABS can be operated with N_{ABS} different spin state modes and the detector count rate is measured for all possible N_{BRP} transition states, then $N_{\text{BRP}} \cdot N_{\text{ABS}}$ equations are obtained. For calibration it is necessary to determine $N_{\text{eff}} + N_{\text{hfs}} \cdot N_{\text{ABS}}$ unknowns, that are the N_{hfs} hfs population numbers for of all N_{ABS} spin state modes plus the N_{eff} efficiencies. The degree of freedom N_f is given by

$$N_f = (N_{\text{BRP}} - N_{\text{hfs}}) \cdot N_{\text{ABS}} - N_{\text{eff}} \, . \tag{21}$$

For $N_f \geq 0$ the system of equations which relates the detector count rates to

Symbol	MFT-B	SFT-B	Efficiency	Error
ε_{s14}	-	1-4	99.3	1.34
ε_{s24}	-	2-4	101.0	1.03
$\varepsilon_{m13r12c14}$	1-3	1-4	101.0	1.06
$\varepsilon_{m13r23c14}$			98.6	1.41
$\varepsilon_{m23r12c14}$	2-3	1-4	-1.0	1.13
$\varepsilon_{m23r23c14}$			94.9	1.23
$\varepsilon_{m13r12c24}$	1-3	2-4	99.9	0.42
$\varepsilon_{m13r23c24}$			90.3	0.82
$\varepsilon_{m23r12c24}$	2-3	2-4	0.0	1.10
$\varepsilon_{m23r23c24}$			97.4	1.04

Table 1
The table lists the static magnetic field settings (MFT-B and SFT-B) and efficiencies [%] of the BRP transitions for hydrogen running and a transmission ratio $\frac{\sigma_2}{\sigma_1} = 1.029$. The dependence of the MFT efficiencies on the SFT-B setting is significant for ε_{m13r23}. Further details and the results for deuterium are given in [18,17].

the hfs intensities (4) can be solved for the intensities I_a and the efficiencies entering the matrix M_{ia} [17]. In case of hydrogen, 7 ABS operation modes are typically used for a calibration measurement, which results in $N_f = 39$. In case of deuterium, two calibration schemes are used, one with 5 ABS modes ($N_f = 74$) and one with 6 modes ($N_f = 97$). The numerical method is outlined in App. A and described in detail in [19]. Tab. 1 summarizes the results of a calibration measurement with hydrogen. Calibration measurements are performed periodically to check that the efficiencies are stable in time. No significant change of the efficiencies has been observed during the time the Polarimeter has been operated at HERMES.

4.4 The Sextupole Transmissions

The transmission probabilities of the sextupole system depend on the velocity distribution of the sample beam and thus on the operating temperature of the storage cell. It follows that it is difficult to obtain absolute values for the transmission probabilities. However, as argued at the end of Sec. 4.1, only ratios of the transmission probabilities for different hyperfine states are required for a given operating temperature.

The beam blocker ensures that atoms in states with $m_J = -1/2$ are not able to reach the detector. Therefore only the ratio σ_2/σ_1 is required for hydrogen and σ_2/σ_1 and σ_3/σ_1 for deuterium. Since the critical field of deuterium (11.7 mT) is much smaller than of hydrogen (50.7 mT), the Stern-Gerlach force depends in high field exclusively on m_J so that the ratios σ_2/σ_1 and σ_3/σ_1 for deuterium can assumed to be one. This is confirmed by numerical calculations carried out with an atom tracking program. It follows that the only transmission ratio that has to be measured is σ_2/σ_1 for hydrogen.

The transmission ratio σ_2/σ_1 for hydrogen at the target working point (temperature of about 95 K) was determined by minimizing the χ^2-value of the calibration results. The result shown in the left hand graph of Fig. 7 gives

$$\left.\frac{\sigma_2}{\sigma_1}\right|_{95\,K} = 1.029 \pm 0.0015\,. \tag{22}$$

Since the uncertainty of σ_2/σ_1 is - at the working point - about one order of magnitude below the systematic uncertainty of the transition efficiencies, it is neglected in the error calculation of the polarization.

A possible dependence of the transition efficiencies on the cell temperature is neglected, as the velocity of the transmitted atoms is to a large extent fixed by the sextupole system. Calibration measurements performed at different temperatures agreed with this assumption. Only the efficiency $\varepsilon_{m13r23c24}$ increased

slightly with decreasing temperature. This particular transition is not used for polarization measurements and is ignored. The polarization measurements with hydrogen are performed using five instead of the minimum required four detector count rates to allow a fit of σ_2/σ_1 to the measured data. The result is shown in the right hand graph of Fig. 7. Thus all calibrations required for the calculation of the hfs population numbers and the polarization are obtained experimentally.

5 Conclusions

It has been shown that the polarimeter is able to measure the hfs populations of a thermal atomic beam effusing out of a storage cell with systematic error below 0.01 for each hyperfine state. However the polarization of the effusing beam is in the case of the HERMES target not identical to the effective target polarization as seen by the electron beam. This arises partially because of recombination of atoms in the target cell and the possibility of finite polarization of molecules, and also because a sampling correction has to be applied. This correction takes account of the difference in the number of wall collisions of the atoms within the sample beam and the target cell and of the possibility of a non-uniform surface in the cell and sample tube [4,17].

In the HERMES data taking period of 1997 the time required to measure the polarization P_z of hydrogen with a statistical uncertainty ΔP_z of ± 0.0125 was about $70\,s$ per injection mode. In 1998 when deuterium was in use the

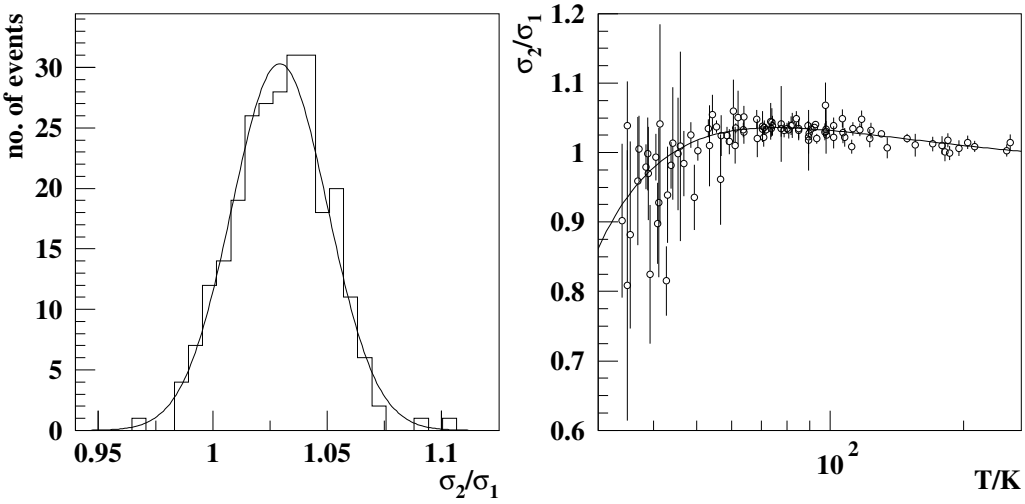

Fig. 7. The left graph shows a histogram of the measured ratio σ_2/σ_1 for hydrogen at $95\,K$ storage cell temperature. The average value is 1.029 ± 0.0015. The right graph shows the measured ratio versus storage cell temperature (open circles) and a polynomial fit to the data (solid line).

statistical precision for a measurement period of 90 s was on average 0.031 for positive and 0.022 for negative vector polarization. In the data taking periods of 1999 and 2000, the uncertainties were similar. These results show that the polarimeter is also a very good instrument for monitoring the polarization. This is important during the optimization of the ABS to obtain maximum target density and polarization and during HERMES data taking for data quality checks. For HERMES data analysis the polarization can be averaged over several runs during a HERA fill because the stability of the HERMES target operation is high. In these circumstances the statistical uncertainty of the polarization measurement is not significant.

The systematic uncertainty $\Delta_{sys}P_z$ in the absolute polarization measurement for hydrogen was on average 0.0075 for positive and 0.009 for negative nuclear polarization over the data taking period of HERMES in 1997. The corresponding systematic uncertainties for deuterium have been 0.011 for positive and 0.0088 for negative nuclear polarization in the data taking period of 1998. The major contribution to these uncertainties is from the efficiencies of the rf-transitions. The efficiencies of the transitions used for the hydrogen polarization measurement were measured to be in the range of $94.9 \pm 1.23 \ldots 101 \pm 1.06\,\%$. The corresponding values for deuterium were $90.8 \pm 1.5 \ldots 99.8 \pm 1.2\,\%$ with the exception of the SFT 3-6 transition with an efficiency of $80.4 \pm 0.9\,\%$. No significant long term change of these efficiencies has been observed during the operation at HERMES. Evidence for this is shown by the polarization data as function of time in Fig. 8. The small fluctuations in this figure are related to known changes in the target oper-

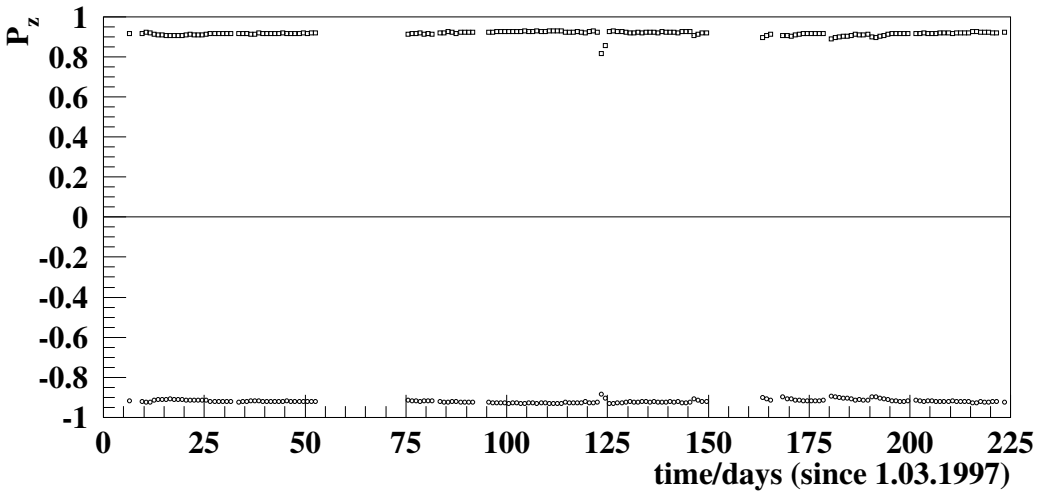

Fig. 8. Proton polarization P_z versus time, measured with the polarimeter during the 1997 run period of HERMES. The target spin direction was reversed every 45 sec and the points are averaged over one day. Therefore two polarization values appear on the plot for each day. The gaps are periods when the target was operating with unpolarized nuclei.

ating conditions. Other possible causes for systematic uncertainties such as the sensitivity of the detector system cancel out provided that there are no significant changes within a measurement cycle which typically takes one or two minutes. The polarimeter has been continuously in operation (except for the HERA shutdown periods) at the HERMES target since 1996, the first two years with hydrogen and since 1998 with deuterium. It is found to be a very reliable instrument.

6 Acknowledgments

We gratefully acknowledge the DESY management for its support and the DESY staff and the staffs of the collaborating institutions. This work was supported by the German Bundesministerium für Bildung, Wissenschaft, Forschung und Technologie (BMBF 056MU22I(1) and 057ER12P(2)); the U.K. Particle Physics and Astronomy Research Council; the U.S. Department of Energy and the National Science Foundation; the Dutch Foundation for Fundamenteel Onderzoek der Materie (FOM) and the Italian Instituto Nazionale di Fisica Nucleare (INFN).

A The Least Square Fit Algorithm for the Evaluation of a Calibration

This section is a summary of the least square fit algorithm used for the calibration and is described in detail in [19].

In order to evaluate a calibration measurement, one defines the vector $\mathbf{x}$ of parameters (efficiencies ε and hfs intensities $\mathbf{I}$) by $\mathbf{x} = (\varepsilon, \mathbf{I})^T$. The measured values are collected in a vector η, which deviates from the real values $\mathbf{y} = S_a$ by the statistical error, which is described by the covariance matrix C_y. Eqn. 4 has then to be rewritten in the form

$$f_a(\mathbf{x}, \mathbf{y}) = \sum_b M_{ab}(\varepsilon) \cdot I_b - S_a = 0 \tag{A.1}$$

Eqn. A.1 is then approximated using the first order term of the Taylor series around $\mathbf{x}_0$ and $\mathbf{y}_0$ respectively

$$\mathbf{f}(\mathbf{x}, \mathbf{y}) = \mathbf{f}(\mathbf{x}_0, \mathbf{y}_0) + A\,(\mathbf{x} - \mathbf{x}_0) + B\,(\mathbf{y} - \mathbf{y}_0) = 0\,, \tag{A.2}$$

where the matrices A and B contain the partial derivatives

$$a_{kl} = \left(\frac{\partial f_k}{\partial x_l}\right)_{\mathbf{x}_0,\mathbf{y}_0} \qquad b_{kl} = \left(\frac{\partial f_k}{\partial y_l}\right)_{\mathbf{x}_0,\mathbf{y}_0} . \tag{A.3}$$

According to Eqn. A.1, B is the negative unit matrix. The covariance matrices C_x and $C_B = G_B^{-1}$ are defined by

$$\begin{aligned} C_B &= B\, C_y\, B^T = C_y \\ C_x &= (A^T\, G_B\, A)^{-1} = (A^T\, C_y^{-1}\, A)^{-1} \end{aligned} \tag{A.4}$$

If $\mathbf{x}_0$ and $\mathbf{y}_0$ are the initial estimations of $\mathbf{x}$ and $\mathbf{y}$, the one obtains improved estimations $\mathbf{x}_1$ and $\mathbf{y}_1$ with

$$\mathbf{x}_{k+1} = \mathbf{x}_k + \delta\mathbf{x}_k \qquad \mathbf{y}_{k+1} = \mathbf{y}_k + \delta\mathbf{y}_k\,, \tag{A.5}$$

where

$$\begin{aligned} \delta\mathbf{x}_k &= -C_x\, A^T\, C_y^{-1}\, \mathbf{f}(\mathbf{x}_k, \mathbf{y}_k) \\ \delta\mathbf{y}_k &= \mathbf{f}(\mathbf{x}_k, \mathbf{y}_k) + A\, \delta\mathbf{x}_k\,. \end{aligned} \tag{A.6}$$

The covariance matrix C_x has the following form

$$C_x = \begin{pmatrix} C_\varepsilon & C_{\varepsilon,I} \\ C_{I,\varepsilon} & C_I \end{pmatrix}\,, \tag{A.7}$$

so that the covariance matrix C_ε is only a part of C_x. It contains the uncertainties and covariances of the efficiencies and is used to determine the systematic uncertainty of the polarization measurements. These uncertainties are of statistical nature, but they are used for the calculation of the systematic uncertainty of the polarization measurements.

The covariance matrix $C_{I,syst}$ of the systematic uncertainty of the hfs intensities I_a is given by:

$$C_{I,syst} = T_\varepsilon C_\varepsilon T_\varepsilon^T\,, \tag{A.8}$$

where the matrix T_ε describes the dependence of the evaluated intensities I_a

on the efficiencies ε:

$$(T_\varepsilon)_{kl} = \left(\frac{\partial I_k}{\partial \varepsilon_l}\right) = \sum_j \left(\frac{\partial I_k}{\partial S_j}\right) \cdot \left(\frac{\partial S_j}{\partial \varepsilon_l}\right) . \tag{A.9}$$

The first matrix on the right is identical to R, the inverse of the measurement matrix M:

$$R_{kj} = \frac{\partial I_k}{\partial S_j} . \tag{A.10}$$

Since the matrix elements of M are either independent or linear in every single efficiency ε_l, the matrix A_ε can be calculated from M by the following equation

$$(A_\varepsilon)_{jl} = \frac{\partial S_j}{\partial \varepsilon_l} = \sum_k \left(M_{jk}(\varepsilon_1, \ldots, \varepsilon_l + 1, \ldots, \varepsilon_n) - M_{jk}(\varepsilon_1, \ldots, \varepsilon_l, \ldots, \varepsilon_n)\right) \cdot I_k \, . \tag{A.11}$$

The error propagation of the systematic error can then be treated in the same way as described for the statistical covariance matrix C_I above.

References

[1] HERMES-Proposal, HERMES Collaboration 1990; DESY-PRC-90/91.

[2] HERMES Technical Design Report, HERMES Coll. 1993; DESY-PRC 93/06.

[3] H.-G. Gaul and E. Steffens; Nucl. Instr. Meth. A 316 (1992), 297-305.

[4] A. Airapetian *et al.*; Phys. Lett. B442 (1998), 484-492.

[5] W. Haeberli; Ann. Rev. Nucl. Sci. Vol. 37 (1967), 373-427.

[6] C. Audoin, M. Desaintfuscien and J.P. Schermann; Nucl. Instr. Meth. 69 (1969), 1-10.

[7] P. Schiemenz *et al*; Nucl. Instr. Meth. A 305 (1991), 15.

[8] J. Stewart *et al* in: 6th Int. Workshop on Pol. Beams and Pol. Gas Targets, Cologne 1995; World Scientific 1996.

[9] R. Gilman *et al*; Phys. Rev. Lett. 65 (1990), 1733-1736.

[10] F. Stock *et al.*; Nucl. Instr. Meth. A 343 (1994), 334-342.

[11] H. Kolster; Ph.D. Thesis, LMU München 1998.

[12] B. Braun; Ph.D. Thesis, LMU München 1995.

[13] W. Drewes, H. Jänsch, E. Koch and D. Fick; Phys. Rev. Let. 50 (1983), 1759-1762.

[14] N.F. Ramsey; Molecular Beams, Clarendon Press, Oxford 1956.

[15] A. Abragam; The Principles Of Nuclear Magnetism, Clarendon Press, Oxford 1961.

[16] R.J. Philpott; Nucl. Instr. Meth. A 259 (1987), 317-323.

[17] C. Baumgarten; Ph.D. Thesis, LMU München 2000.

[18] M. Henoch; Diploma Thesis, Universität Münster 1998.

[19] S. Brandt; Datenanalyse, BI-Wissenschaftsverlag 1992.

[20] A. Metz; Diploma Thesis; LMU München 1995.